Bulk and monolayer As_2S_3 as promising thermoelectric material with high conversion performance

Abhishek Patel[a,*], Deobrat Singh[b,*], Yogesh Sonvane[c], P.B. Thakor[a], Rajeev Ahuja[b,d,*]

[a] Department of Physics, Veer Narmad South Gujarat University, Surat 395007, India
[b] Condensed Matter Theory Group, Materials Theory Division, Department of Physics and Astronomy, Uppsala University, Box 516, 75120 Uppsala, Sweden
[c] Department of Applied Physics, S.V. National Institute of Technology, Surat 395007, India
[d] Applied Materials Physics, Department of Materials and Engineering, Royal Institute of Technology (KTH), S-100 44 Stockholm, Sweden

ARTICLE INFO

ABSTRACT

The electronic and thermoelectric properties of recently synthesized As_2S_3 in the form of 2D by experiment have been investigated in this work. The thermoelectric properties of As_2S_3 has been studied by the first-principles calculations and the Boltzmann Transport theory. The result shows that As_2S_3 has indirect band gap of 2.31 eV for monolayer and 2.08 eV for bulk. From phonon dispersion spectra, both bulk and monolayer have dynamical stability. The Seebeck coefficient (S) as a function of temperature is investigated for monolayer and bulk of As_2S_3 and its values at 300 K temperature are 188 and 298 μV/K. Also, the values of S are drastically decreasing when temperature increases in bulk As_2S_3 while in case of monolayer As_2S_3, the values of S have less variation with increasing temperature. The electronic figure of merit (ZT_e) for bulk As_2S_3 is found to be 5.04 at 300 K while at higher temperature ZT_e values significantly reduced to 3.76. For monolayer As_2S_3, the electronic figure of merit, ZT_e is also showed higher value of 1.84 at 300 K and at higher temperature it has ~ 2.75. These investigation shows that the bulk and monolayer have new materials for the potential applications in the thermoelectric devices.

1. Introduction

The rapid growth in the world's energy demand have become global problem from past few decades. Recently, this demand is satisfying by fossil fuels and other non-renewable sources.[1] The large consumption of these sources produces shortage of fuel in the nearest future and negative impact on the environment. Almost the burning process of fossil fuel produce energy with waste heat and exhaust gas released into the atmosphere, which cause air-pollution in environment.[2,3] The thermoelectric materials are desirable solution to produce electricity from the waste heat and useful as solid-state Peltier coolers.[4,5] To develop and identify such materials with high thermoelectric efficiency more than available at present remains is a challenge task.[6,7]

The thermoelectric device has ability to convert the temperature gradient into the electric potential[8]. This ability can be summarized as a figure of merit (ZT) which depends upon Seebeck coefficient, thermal and electrical conductivities of material and temperature. Generally, the figure of merit of the material is expressed by $ZT = S^2\sigma T/\kappa$; where, S, σ and κ represent Seebeck coefficient, electrical conductivity and κ thermal conductivity.[6,9] The thermal conductivity

$\kappa = \kappa_e + \kappa_1$ in which κ_e the electronic thermal conductivity and κ_λ represents the electronic thermal conductivity and the lattice thermal conductivity, respectively.[9] The material with large value of ZT have better performance in conversion of heat into electricity.[10] The higher value of power factor (which is $S^2\sigma$) and lower value of thermal conductivity are fundamental necessaries to improve the value of ZT. [11] The best thermoelectric materials reported to till present time have been measured at ZT values of around 2.5 to 2.8.[12–14] Recently, Scientists at TU Wien have developed new material (thin layer of iron, vanadium, tungsten and aluminium applied to a silicon crystal) with ZT value lies between 5 and 6.[15] The chalcogenide material is good source of thermoelectric material due to high Seebeck coefficient and lower thermal conductivity.[16] Sulfide materials are import members of this chalcogenide family. So, these materials have a lot of attraction of research in this era. [17–19]

Nowadays, 2D layered materials have extraordinary properties for the potential applications in the field of nanoelectronics, photocatalysis, and energy systems such as solar cell, thermoelectric devices. [20–24] As_2X_3 (where X = S, Se and Te) based monoclinic structures are bulk-layered materials, and it has highly anisotropic material

---

family. The layered form of As_2S_3 is successfully experimentally synthesize by Siskins et al.[25] in which the layered form of As_2S_3 shows wonderful chemical stability, high anisotropic mechanical and optical properties. The layered As_2S_3 is semiconducting material with these remarkable properties. We will discuss about the theoretical work to calculate the structural, electronic and thermoelectric properties of bulk and monolayer As_2S_3 material. Also, for the dynamical stability, the phonon dispersion spectra are calculated. For simulating thermoelectric properties, the Seebeck coefficient, electrical conductivity, electronic thermal conductivity and electronic figure of merit have been computed. The material studied here shows the high thermoelectric performance.

2. Computational methods

The Vienna Ab-initio Simulation Package (VASP) code have been used to simulate the Density Functional Theory calculations in the present work.[26–28] The Generalized Gradient Approximation (GGA) method within the Perdew − Burke − Ernzerhof (PBE) functional has been employed. [29] These calculations performed within the energy convergence criterion of 10^{-8} eV with a plane-wave cut-off energy of 500 eV for both, monolayer and bulk As_2S_3 systems. In the As_2S_3 monolayer system, the high vacuum of 20 Å along normal direction was inserted to prevent interactions with adjacent layers.[30–32] The Monkhorst-Pack k-point meshes $(7 \times 1 \times 7)$ and $(7 \times 7 \times 7)$ have been used for monolayer and bulk As_2S_3, respectively.[33] The conjugate gradient (CG) method with the Hellmann-Feynman forces converge criterion of 0.001 eV/Å is used to optimize the structure. The density Functional perturbation theory (DFPT) calculations were carried out for $(2 \times 2 \times 3)$ sized supercell of As_2S_3 bulk-material and $(3 \times 1 \times 3)$ sized supercell of monolayer material of As_2S_3. By using this DFPT results, the Phonopy code has been employed to determine the phonon dispersion for both phases of As_2S_3, monolayer and bulk. [34] The Constant Relaxation Time Approximation (CRTA) and Boltzmann Transportation Equation (BTE) is implemented in BoltzTraP2 code used to calculate the thermoelectric properties.[35,36] For the appropriate and powerful visualization of As_2S_3 material, the VESTA software has been employed.[37]

3. Results and discussion

3.1. Structural properties of monolayer and bulk As_2S_3 material

Energy minimized structure of monolayer and bulk As_2S_3 have been illustrated in the Fig. 1. They have monoclinic lattice arrangement. The monolayer As_2S_3 contains two formula units of As_2S_3 due to the octet rule. Here, As atoms have 3 coordinates (3 As-S bonds) and S atoms

Table 1
Calculated the lattice parameters and angles of bulk and monolayer As_2S_3.

Material	a (Å)	b (Å)	c (Å)	α	β	γ
As_2S_3 (monolayer)	4.6576	–	12.2425	89.94°	112.39°	90.11°
As_2S_3 (bulk)	4.6014	11.0069	12.2554	90°	111.73°	90°

have 2 coordinates (2 As-S).[38,39] The primitive unit-cell of bulk As_2S_3 contains two monolayer As_2S_3.

After structure optimization of As_2S_3 material, the lattice constants of monolayer As_2S_3 are a = 4.6576 Å and c = 12.2425 Å. The high vacuum of 20 Å is also present in the c direction to prevent interactions of adjacent layers. While for bulk phase of As_2S_3, the lattice constants are a = 4.6014 Å, =11.0069 Å and c = 12.2554 Å. The lattice constants in a and c direction are very close to those of bulk structure as shown in Table 1. The experimental measured values of bulk As_2S_3 are 4.22 and 11.46 in a and c directions. Our optimized structures of As_2S_3 for bulk and monolayer phase are very close to previous investigations. [38,39]

3.2. Electronic properties and phonon dispersion of As_2S_3

To examine the electronic properties of arsenic tri-sulfide, As_2S_3, the electronic band-structure along the high symmetry path $\Gamma − z− C− Y− \Gamma$ points is computed for both phase, bulk and monolayer. The Fig. 2 (a, c) illustrates the electronic band-structure of As_2S_3 for monolayer and bulk phase. The indirect band gap of monolayer As_2S_3 and bulk As_2S_3 are calculated to be 2.31 eV and 2.08 eV, respectively (see Table 2). The bulk and its monolayer of As_2S_3 has semiconducting nature. The indirect band gap is found from Y-point in valence band to Γ-point in conduction band in monolayer and bulk As_2S_3. The direct bandgap is slightly larger than the indirect electronic bandgap. These results of the electronic band structures within the PBE functional are good agree with the previous investigations.[38]

Further, the phonon calculations were performed along the $\Gamma − z− C− Y− \Gamma$ high symmetry directions for dynamical stability of the As_2S_3 monolayer and bulk. The Fig. 2(b, d) shows the phonon dispersion of As_2S_3 for monolayer and bulk phase. Both bulk and monolayer As_2S_3 systems are free from imaginary frequencies. The positive values of frequency in phonon dispersion of monolayer and bulk structure have showed their dynamical stabilities.

To better analysis of the electronic band-structures, the projected density of states (PDOS) of monolayer As_2S_3 and bulk As_2S_3 have determined as shown in Fig. 3. It is observed that the p-orbital of S atom is mainly contributed near the Fermi level (E_F) and a small contribution comes from p-orbital of As atoms in the valence band maximum (VBM).
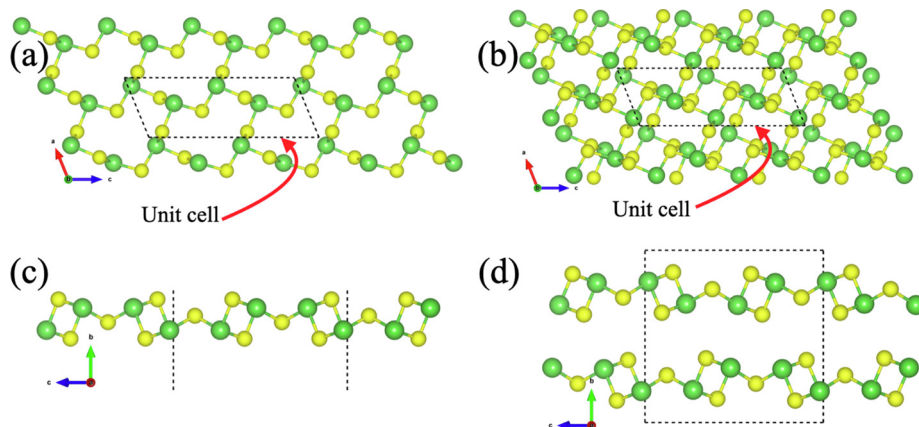

Fig. 1. (a) Top view of monolayer As_2S_3 and (b) top view of bulk As_2S_3, (c) side view of monolayer As_2S_3, (d) unit-cell of bulk As_2S_3. The dotted line shows the unit cell of monolayer and bulk As_2S_3. The green and yellow colour represents the arsenic and sulfur atoms, respectively.
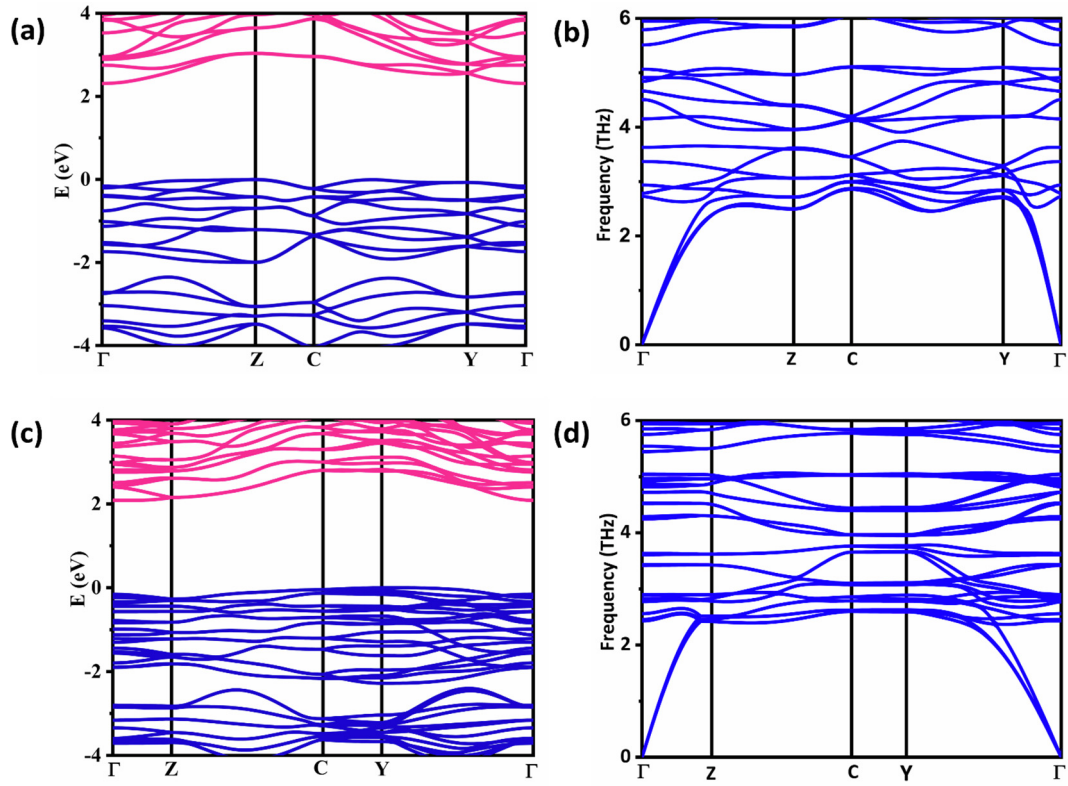
Fig. 2. (a) Electronic band-structure of monlayer-As_2S_3 (b) phonon-dispersion of monolayer-As_2S_3 (c) Electronic band-structure of bulk-As_2S_3 and (d) phonon-dispersion of bulk-As_2S_3.

Table 2
Calculated electronic band gaps in monolayer and bulk As_2S_3.

Material	Phase	Structure	Indirect Bandgap	Direct Bandgap
As_2S_3	monolayer	monoclinic	2.309 eV	2.471 eV
As_2S_3	bulk	monoclinic	2.084 eV	2.241 eV

In the conduction band minimum (CBM), the p-orbital of As atom is strongly hybridized with p-orbital of S atom as presented in Fig. 3(a). Similar contribution is found to be in the bulk As_2S_3 system like monolayer As_2S_3 as shown in Fig. 3(b). From the electronic band structures, it is also observed that the flat band lines present at the top of the valence band as shown in Fig. 2(a, c). The flat band lines have large effective mass and the Seebeck coefficient is directly proportional to the effective mass (i.e. S α m*). According to that the bulk and its monolayer have higher values of Seebeck coefficient. Due to the

relatively flatter band lines in bulk system as compare to monolayer of As_2S_3 system has higher Seebeck coefficient which is shown in next section.

3.3. Thermoelectric properties of As_2S_3 material

The thermoelectric component, such as the Seebeck coefficient, electrical conductivity and electronic thermal conductivity, and electronic figure of merit, ZT_e have been calculated as functions of temperature. Additionally, constant relaxation time approximation with $\tau = 10^{-14}$ s, which is used to calculate the thermal and electrical conductivity. Fig. 4 (a) shows computed Seebeck coefficient of As_2S_3 for temperature range 300 K to 1200 K. These materials show higher value of Seebeck coefficient at room temperature. As the temperature increases, the Seebeck coefficient decreases gradually. The Seebeck coefficient of bulk As_2S_3 remains higher than monolayer because
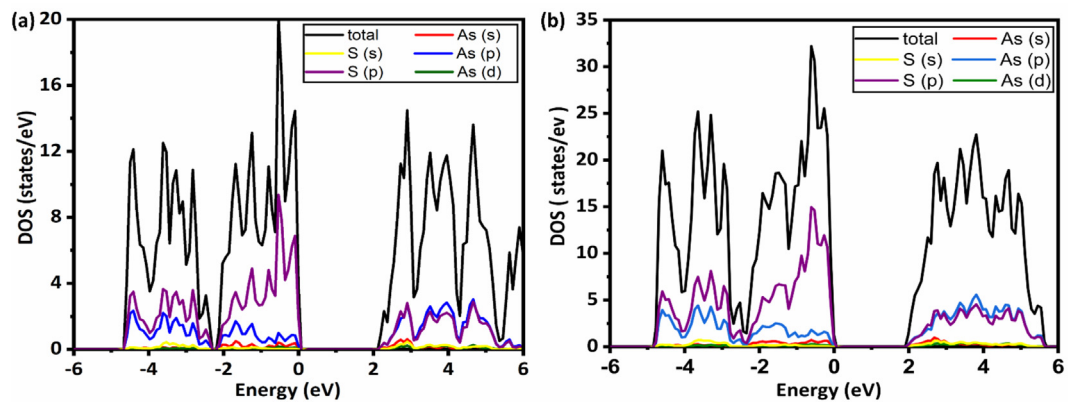

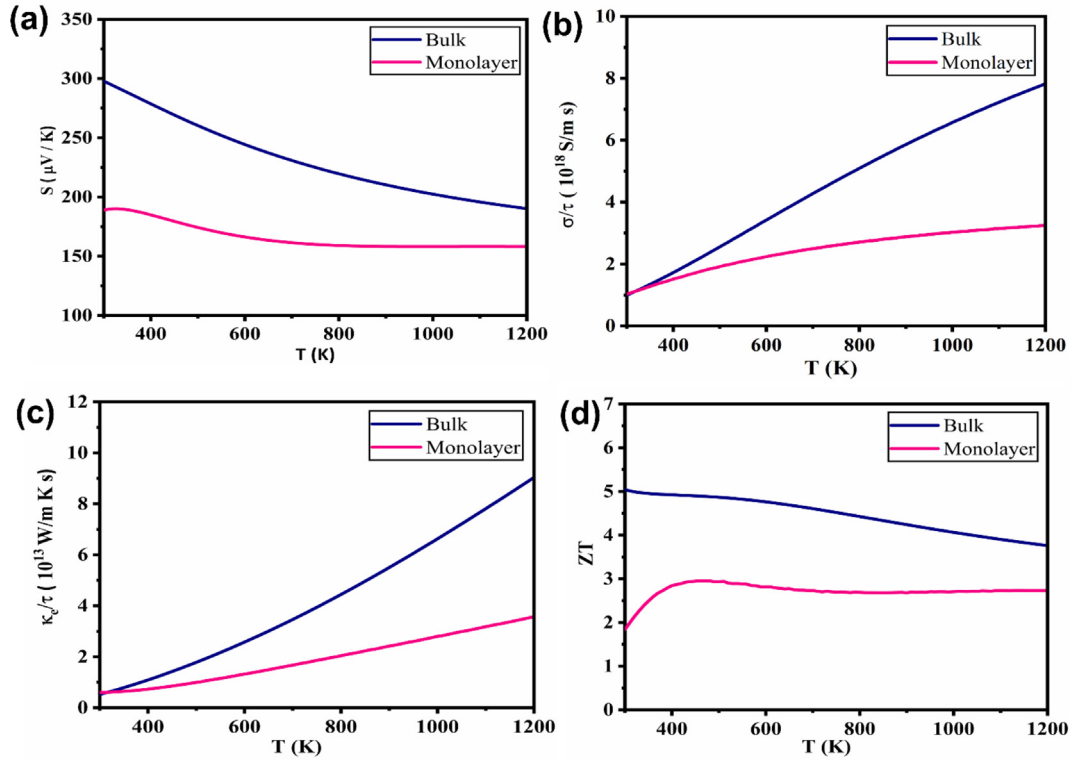Fig. 3. (a) DOS of monolayer- As_2S_3, (b) DOS of bulk- As_2S_3.

Fig. 4. (a) Seebeck Coefficients, (b) electrical conductivity (c) electronic thermal conductivity and (d) Figure of Merit of As_2S_3.

Table 3
Seebeck coefficients (S) and electronic figure of merit (ZT_e) of As_2S_3.

Temperature(K)	As_2S_3 (Monolayer)		As_2S_3 (Bulk)	
	S (μV/K)	ZT_e	S (μV/K)	ZT
300	188.92	1.84	291.81	5.04
500	174.28	2.93	260.29	4.87
800	159.08	2.69	219.61	4.42
1000	158.15	2.71	202.41	4.06
1200	158.12	2.73	190.19	3.76

layered form of As_2S_3 have low effective mass due to the flatter band lines as compare to bulk form. But this difference is also decrease with increment of temperature. The values of Seebeck coefficient at room temperature are found to be 188.92 μV/K and 291.81 μV/K for monolayer and bulk As_2S_3, respectively. Moreover, the values of Seebeck coefficient have almost same at higher temperature see Table 3. It means that it works very well at lower as well as higher temperature.

Fig. 4 (b) and (c) shows electrical conductivity and electronic thermal conductivity as a function of temperature at constant relaxation time. For thermal and electronic conductivities, the initial value at room temperature are same for both bulk and monolayer phase of As_2S_3. We know that the charge density is also function of temperature. It means that the charge density will increases when temperature increases and it will get more thermal energy to release free electrons from valence band into the conduction band. As a consequence, the excited electrons converted into charge carriers which shows increasing behaviors with temperature. We can see that the values for bulk phase is rapidly increase than monolayer with increase in temperature.

In the monolayer phase, the electrical conductivity is only 1.03×10^{18} S/ m s at 300 K. Then, it is increased with temperature and reached 3.25×10^{18} S/ m s at 1200 K. Similarly, for bulk phase, it is initial value 0.996×10^{18} S/ m s at 300 K, which is almost same with bulk phase. But it is increased more rapidly than monolayer phase and reached 7.82×10^{18} S/ m s. This value is much more than two times of

that of monolayer As_2S_3.

Similar, the electrical thermal conductivity is 0.526×10^{13} W/mKs and 0.599×10^{13} W/mKs at 300 K for monolayer and bulk phase of As_2S_3, respectively. Initially, the value of electronic thermal conductivity (κ_e) for monolayer phase is much more than that of bulk. The value of electronic thermal conductivity is increases with temperature for both phases. At the 1200 K, its value is 3.57×10^{13} W/mKs and 9.04×10^{13} W/mKs for monolayer and bulk phase, respectively. The value for bulk Phase is three times more than monolayer phase.

The electronic figure of merit (ZT_e) is efficient way to measure the thermoelectric conversion performance of material. The bulk As_2S_3 have high electronic figure of merit, which is varies from 5.04 to 3.76 for temperature range from 300 K to 1200 K. The ZT_e value of monolayer As_2S_3 is 1.84 at room temperature 300 K as shown in Table 3. Initially, it increases with temperature. Then, it becomes almost constant with temperature for higher value of temperature. It reported ZT_e value 2.73 at 1200 K temperature. At higher temperature, the ZT_e value is remained unchanged with temperature for monolayer As_2S_3. So, the monolayer As_2S_3 have stability in thermoelectric conversion at higher temperature. But this stability is not observed in ZT_e of bulk at higher temperature. It was reported that the values of ZT in previous investigations are 4.6 monolayer α-Te,[3] 2.45 in graphene nanoribbon, [40] penta-PdTe2 reaches 2.42,[41] monolayer InP3 is found to be as high as 2.06,[42] 3.27 in single-layered SnSe,[43] 2 for single-layered SiSb.[44] But bulk As_2S_3 have high thermoelectric performance due to its high ZT_e value. Based on above calculations, the bulk As_2S_3 and monolayer As_2S_3 can be proposed as promising candidates for thermoelectric applications.

4. Conclusions

The electronic, vibrational and thermoelectric properties of As_2S_3 for monolayer and bulk phase are systematically determined using the first-principles calculations. From the phonon dispersion, the dynamical stability of the material is proved. This material shows indirect bandgap

2.31 eV for monolayer phase and 2.08 eV for bulk-phase. From thermoelectric computation, the monolayer As_2S_3 and bulk As_2S_3 have 188.92 μV/K and 291.81 μV/K Seebeck coefficients at 300 K temperature, respectively. The monolayer phase of this material has high electronic figure of merit ZT_e = 1.84 at room temperature and 2.73 at higher temperature. For bulk phase, its ZT_e value varies from 3.76 to 5.04. Bulk As_2S_3 have very high electronic figure of merit ZT_e = 5.04 at 300 K and 3.76 at 1200 K. The finding results suggest that the As_2S_3 material can be utilized in thermoelectric devices.

CRediT authorship contribution statement

A.P.: Methodology, Software, Investigation, Writing - original draft. **D.S.:** Writing - review & editing, Validation. **Y.S.:** Validation. **P.B.T.:** Validation, Supervision. **R.A.:** Validation.

Declaration of Competing Interest

The authors declare that they have no known competing financial interests or personal relationships that could have appeared to influence the work reported in this paper.

Acknowledgements

References

[1] L. Yang, Z.G. Chen, M.S. Dargusch, J. Zou, High Performance Thermoelectric Materials: Progress and Their Applications, Adv. Energy Mater. 8 (2018) 1701797.

[2] F. Perera, Pollution from fossil-fuel combustion is the leading environmental threat to global pediatric health and equity: Solutions exist, Int. J. Environ. Res. Public Health. 15 (2018).

[3] X. Jiang, L. Zhu, B. Li, K. Yao, Thermoelectric properties of monolayer α-Te: Low lattice thermal conductivity and extremely high dimensionless figure of merit, Phys. Lett. Sect. A Gen. At. Solid State Phys. 384 (2020) 126222.

[4] S. LeBlanc, Thermoelectric generators: Linking material properties and systems engineering for waste heat recovery applications, Sustain. Mater. Technol. 1 (2014) 26–35.

[5] R.A. Kishore, A. Nozariasbmarz, B. Poudel, M. Sanghadasa, S. Priya, Ultra-high performance wearable thermoelectric coolers with less materials, Nat. Commun. 10 (2019) 1765.

[6] G.J. Snyder, E.S. Toberer, Complex thermoelectric materials, Nat. Mater. 7 (2008) 105–114.

[7] R. Freer, A.V. Powell, Realising the potential of thermoelectric technology: A Roadmap, J. Mater. Chem. C. 8 (2020) 441–463.

[8] Z.B. Tang, Y.D. Deng, C.Q. Su, W.W. Shuai, C.J. Xie, A research on thermoelectric generator's electrical performance under temperature mismatch conditions for automotive waste heat recovery system, Case Stud. Therm. Eng. 5 (2015) 143–150.

[9] P. Mishra, D. Singh, Y. Sonvane, R. Ahuja, Two-dimensional boron monochalcogenide monolayer for thermoelectric material, Sustain. Energy Fuels. 4 (2020) 2363–2369.

[10] X. Zhang, L.D. Zhao, Thermoelectric materials: Energy conversion between heat and electricity, J. Mater. 1 (2015) 92–105.

[11] J. Li, Z. Ma, R. Sa, K. Wu, Improved thermoelectric power factor and conversion efficiency of perovskite barium stannate, RSC Adv. 7 (2017) 32703–32709.

[12] D. Beretta, N. Neophytou, J.M. Hodges, M.G. Kanatzidis, D. Narducci, M. Martin-Gonzalez, M. Beekman, B. Balke, G. Cerretti, W. Tremel, A. Zevalkink, A.I. Hofmann, C. Müller, B. Dörling, M. Campoy-Quiles, M. Caironi, Thermoelectrics: From history, a window to the future, Mater. Sci. Eng. R Reports. 138 (2019) 100501.

[13] E. Nshimyimana, S. Hao, X. Su, C. Zhang, W. Liu, Y. Yan, C. Uher, C. Wolverton, M.G. Kanatzidis, X. Tang, Discordant nature of Cd in GeTe enhances phonon scattering and improves band convergence for high thermoelectric performance, J. Mater. Chem. A. 8 (2020) 1193–1204.

[14] L.D. Zhao, S.H. Lo, Y. Zhang, H. Sun, G. Tan, C. Uher, C. Wolverton, V.P. Dravid, M.G. Kanatzidis, Ultralow thermal conductivity and high thermoelectric figure of merit in SnSe crystals, Nature. 508 (2014) 373–377.

[15] B. Hinterleitner, I. Knapp, M. Poneder, Y. Shi, H. Müller, G. Eguchi, C. Eisenmenger-Sittner, M. Stöger-Pollach, Y. Kakefuda, N. Kawamoto, Q. Guo, T. Baba, T. Mori, S. Ullah, X.Q. Chen, E. Bauer, Thermoelectric performance of a metastable thin-film Heusler alloy, Nature. 576 (2019) 85–90.

[16] F. Tesfaye, An Overview of Advanced Chalcogenide Thermo-electric Materials and Their Applications, J. Electron. Res. Appl. 2 (2018) 28–41.

[17] Y. Yu, M. Cagnoni, O. Cojocaru-Mirédin, M. Wuttig, Chalcogenide Thermoelectrics Empowered by an Unconventional Bonding Mechanism, Adv. Funct. Mater. 30 (2020) 1904862.

[18] Z.H. Ge, L.D. Zhao, D. Wu, X. Liu, B.P. Zhang, J.F. Li, J. He, Low-cost, abundant binary sulfides as promising thermoelectric materials, Mater. Today. 19 (2016) 227–239.

[19] S. Skipidarov, M.M. Nikitin, Novel Thermoelectric Materials and Device Design Concepts, Nov. Thermoelectr. Mater. Device Des, Concepts, 2019.

[20] A.S. Pawbake, J.O. Island, E. Flores, J.R. Ares, C. Sanchez, I.J. Ferrer, S.R. Jadkar, H.S.J. Van Der Zant, A. Castellanos-Gomez, D.J. Late, Temperature-Dependent Raman Spectroscopy of Titanium Trisulfide (TiS_3) Nanoribbons and Nanosheets, ACS Appl. Mater. Interfaces. 7 (2015) 24185–24190.

[21] F. Bonaccorso, L. Colombo, G. Yu, M. Stoller, V. Tozzini, A.C. Ferrari, R.S. Ruoff, V. Pellegrini, Graphene, related two-dimensional crystals, and hybrid systems for energy conversion and storage, Science 80 (347) (2015) 1246501.

[22] P. Kumar, H. Abuhimd, W. Wahyudi, M. Li, J. Ming, L.-J. Li, Review—Two-Dimensional Layered Materials for Energy Storage Applications, ECS J. Solid State Sci. Technol. 5 (2016) 3021–3025.

[23] H. Li, Y. Shi, M.H. Chiu, L.J. Li, Emerging energy applications of two-dimensional layered transition metal dichalcogenides, Nano Energy. 18 (2015) 293–305.

[24] C. Marichy, M. Bechelany, N. Pinna, Atomic layer deposition of nanostructured materials for energy and environmental applications, Adv. Mater. 24 (2012) 1017–1032.

[25] M. Šiškins, M. Lee, F. Alijani, M.R. Van Blankenstein, D. Davidovikj, H.S.J. Van Der Zant, P.G. Steeneken, Highly Anisotropic Mechanical and Optical Properties of 2D Layered As_2S_3 Membranes, ACS Nano. 13 (2019) 10845–10851.

[26] G. Kresse, J. Furthmüller, Efficient iterative schemes for ab initio total-energy calculations using a plane-wave basis set, Phys. Rev. B - Condens. Matter Mater. Phys. 54 (1996) 11169–11186.

[27] G. Kresse, J. Furthmüller, Efficiency of ab-initio total energy calculations for metals and semiconductors using a plane-wave basis set, Comput. Mater. Sci. 6 (1996) 15–50.

[28] D. Joubert, From, ultrasoft pseudopotentials to the projector augmented-wave method, Phys. Rev. B - Condens. Matter Mater. Phys. 59 (1999) 1758–1775.

[29] J.P. Perdew, K. Burke, M. Ernzerhof, Generalized gradient approximation made simple, Phys. Rev. Lett. 77 (1996) 3865–3868.

[30] Y. Xu, Y. Li, X. Chen, C. Zhang, R. Zhang, P. Lu, First-principle study of hydrogenation on monolayer MoS2, AIP Adv. 6 (2016) 75001.

[31] H. Li, C. Tsai, A.L. Koh, L. Cai, A.W. Contryman, A.H. Fragapane, J. Zhao, H.S. Han, H.C. Manoharan, F. Abild-Pedersen, J.K. Nørskov, X. Zheng, Activating and optimizing MoS_2 basal planes for hydrogen evolution through the formation of strained sulphur vacancies, Nat. Mater. 15 (2016) 48–53.

[32] E.N. Voronina, L.S. Novikov, Ab initio study of unzipping processes in carbon and boron nitride nanotubes under atomic oxygen impact, RSC Adv. 3 (2013) 15362–15367.

[33] H.J. Monkhorst, J.D. Pack, Special points for Brillouin-zone integrations, Phys. Rev. B. 13 (1976) 5188–5192.

[34] A. Togo, I. Tanaka, First principles phonon calculations in materials science, Scr. Mater. 108 (2015) 1–5.

[35] G.K.H. Madsen, J. Carrete, M.J. Verstraete, BoltzTraP2, a program for interpolating band structures and calculating semi-classical transport coefficients, Comput. Phys. Commun. 231 (2018) 140–145.

[36] G.K.H. Madsen, D.J. Singh, BoltzTraP. A code for calculating band-structure dependent quantities, Comput. Phys. Commun. 175 (2006) 67–71.

[37] K. Momma, F. Izumi, VESTA 3 for three-dimensional visualization of crystal, volumetric and morphology data, J. Appl. Crystallogr. 44 (2011) 1272–1276.

[38] B. Mortazavi, F. Shojaei, M. Azizi, T. Rabczuk, X. Zhuang, As_2S_3, As_2Se_3 and As_2Te_3 nanosheets: Superstretchable semiconductors with anisotropic carrier mobilities and optical properties, J. Mater. Chem. C. 8 (2020) 2400–2410.

[39] N. Morimoto, The crystal structure of orpiment (As_2S_3) refined, Mineral. J. 1 (1954) 160–169.

[40] H. Sadeghi, S. Sangtarash, C.J. Lambert, Enhancing the thermoelectric figure of merit in engineered graphene nanoribbons, Beilstein J. Nanotechnol. 6 (2015) 1176–1182.

[41] Y.S. Lan, X.R. Chen, C.E. Hu, Y. Cheng, Q.F. Chen, Penta-PdX₂ (X = S, Se, Te) monolayers: Promising anisotropic thermoelectric materials, J. Mater. Chem. A. 7 (2019) 11134–11142.

[42] T. Ouyang, E. Jiang, C. Tang, J. Li, C. He, J. Zhong, Thermal and thermoelectric properties of monolayer indium triphosphide (InP_3): a first-principles study, J. Mater. Chem. A. 6 (2018) 21532–21541.

[43] F.Q. Wang, S. Zhang, J. Yu, Q. Wang, Thermoelectric properties of single-layered SnSe sheet, Nanoscale. 7 (2015) 15962–15970.

[44] H.H. Huang, X. Fan, D.J. Singh, W.T. Zheng, The thermal and thermoelectric transport properties of SiSb, GeSb and SnSb monolayers, J. Mater. Chem. C. 7 (2019) 10652–10662.